The highly active catalysts of nanocomposite K-Co-CeO_2 for soot combustion

Electronic Supplementary Information

Synthesis of nanocomposite K-Co-CeO_2 catalysts:

K-Co-CeO_2 nanocomposite catalysts were prepared by micropore-diffused co-reaction method (MDC) with the ammonia solution as pH adjusting agent and polyethylene glycol as stabilizing agent. In this work, the catalysts will be generically named as $K_xCo_{0.2}CeO_2$, where x is the molar ratio of K/Ce (x = 0.01, 0.04, 0.1, 0.2, 1). all chemical reagents were purchased from Beijing Chemical Reagent Company in China and all of their purity was analytic grade. All reactant gases were purchased from Dalian Date Standard Gas Company in China and all of their purity was greater than 99.999%.

Figure S1: The digital photos of MDC device. The right photo is the ceramic membrane reactor composed of four ceramic membrane tubes [1], which is the core of the device of MDC method.

Characterization:

The surface morphology of the samples was observed by SEM (S-4800, Hitachi company, Japan). The internal morphology and grain characteristics of the samples were observed by TEM, using a JEOl JEM 2100 electron microscope equipped with a field emission source at an accelerating voltage of 200 kV. For nanocomposite $K_{0.1}Co_{0.2}CeO_2$ catalysts, powders were suspended in methanol for about 5 min under ultrasonic treatment, then deposited on holey carbon-coated grids. X-ray fluorescence (XRF) measurements were carried out on a CSX-1000E spectrometer for determining the actual contents of K, Co and Ce in catalysts. The crystal structures of the fresh catalysts were determined by a powder X-ray diffractometer (Shimadzu XRD 6000) using Cu K_α (λ = 0.15406 nm) radiation with a Nickel filter operating at 40 kV and 10 mA. The diffractometer data were recorded for 2θ values between 10 and 90° at a scanning rate of 4 °/min. XPS spectra were recorded using a Perkin-Elmer PHI 5600 ci spectrometer with a standard Al Kα source (1486.6 eV) working at 350 W. The working pressure was less than $1*10^{-8}$ Pa. The spectrometer was calibrated by assuming the binding energy (BE) of the Au $4f_{7/2}$ line to lie at 84.0 eV with respect to the Femi level. The standard deviation in the BE values of the XPS line is 0.10 eV. The BET specific surface areas were measured with linear parts of the BET plot of

the N_2 isotherms, using a Micromeritics ASAP 2010 analyzer. Raman spectra were performed on LabRAM HR spectrometer manufactured by Horiba Jobin Yvon company, France. The laser excitation wavelength was 514 nm. The UV-Vis DRS experiments were performed on Hitachi U-4100 UV-Vis spectrophotometer with the integration sphere diffuse reflectance attachment. The powder samples were loaded in a transparent quartz cell and were measured in the region of 200 ~ 800 nm at room temperature. Pure $BaSO_4$ was used as reference sample. FT-IR spectra were obtained in the wave number ranging between 6000 ~ 400 cm^{-1} via a FTS-3000 spectrophotometer manufactured by American Digilab company. For the transmission IR experiments under ambient conditions, the measured wafer was prepared as KBr pellet with the weight ratio of sample to KBr, 1/100. The resolution was set at 4 cm^{-1} during measurement.

H_2-TPR measurements were performed in a conventional flow apparatus. 200 mg sample was pretreated at an oxygen atmosphere by calcination at 600°C for 1 h and subsequently cooled to 100°C with helium flowing. Afterwards, 10% H_2/He flow (40 cm^3/min) was passed over the catalyst bed while the temperature was ramped from 100°C to 900°C at a heating rate of 10°C/min. The hydrogen consumption signal was monitored by a thermal conductivity detector (TCD). Before the outlet gases entering the TCD, a cooling trap and a filter packed with molecular sieve 5A (60~80 meshes) were used to remove H_2O and CO_2. In order to investigate the effect of NO_2 on the soot combustion, NO oxidation experiments were carried out by the means of TPO and NO_2 concentrations were detected by Quantachrome autosorb-1C mass spectroscopy. The blank soot (without catalyst) and two typical catalysts (n$mCeO_2$ and $K_{0.1}Co_{0.2}CeO_2$) were used for activity evaluation. The other experimental condition is the same as soot combustion in TPO reaction. NO adsorption on $K_{0.1}Co_{0.2}CeO_2$ catalyst was carried out in the quartz flow reactor using 200 mg sample. The catalyst was pretreated in a gas flow of O_2/He (10% O_2 by volume) at 500 °C for 1 h and then cooled to the experimental temperature. When the temperature had stabilized at 350 °C, 2000 ppm NO and 5% O_2 in He were introduced at a rate of 200 ml/min for 20 min for NO adsorption. The NO concentration was monitored by a Vario Plus gas analyzer (MRU company, Germany).

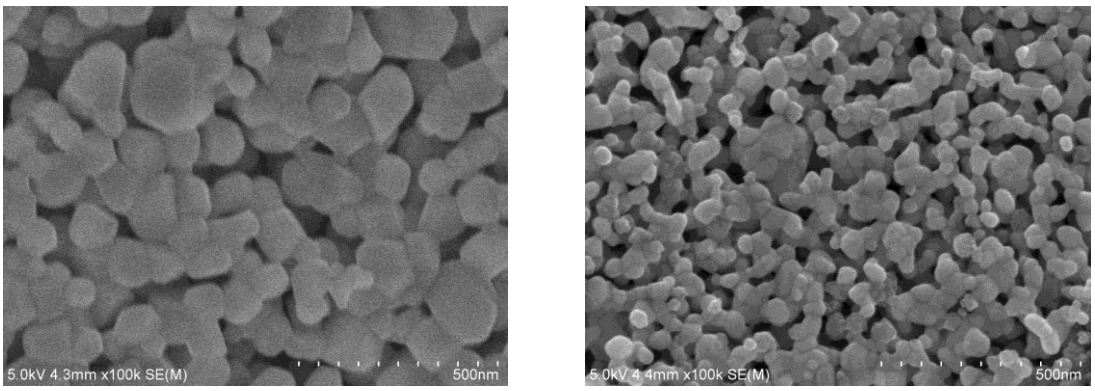

(a) (b)

Figure S2: SEM photographs of the catalysts. (a)$K_{0.01}Co_{0.2}CeO_2$ (b)$K_{0.5}Co_{0.2}CeO_2$

It can be observed that $K_xCo_{0.2}CeO_2$ samples obtain high dispersity. With the increasing of potassium content, the particle sizes of catalysts become smaller and the dispersity become better.

The Co 2p, Ce 3d, and O 1s XPS spectra of some samples are shown in Fig. S3. The Co 2p XPS spectra of Co_3O_4, $Co_{0.2}CeO_2$, and $K_{0.1}Co_{0.2}CeO_2$ samples indicate that the strongest photoelectron signals for cobalt arise from the $2p_{3/2}$ and $2p_{1/2}$ levels. The two XPS peaks of $Co_{0.2}CeO_2$ ($2p_{2/3}$ = 779.9 eV and $2p_{1/2}$ = 795.2 eV) are due to the formation of bulk Co_3O_4. The higher energy positions of Co 2p peaks for $Co_{0.2}CeO_2$ sample compared with Co_3O_4 are ascribed to the existence of more Co^{2+} in the catalysts than that in the bulk Co_3O_4 [2]. In the presence of potassium, the binding energy shifts to the lower position. It is probably because that the addition of K promotes more Co^{3+} formation. In Fig. S3(b), the Ce 3d peak positions agree with the data obtained for $nmCeO_2$. The Ce $3d_{5/2}$ lines, characteristic of the Ce(IV) oxidation state, are located at 882.3, 889.0, and 898.3 eV. The Ce $3d_{3/2}$ lines appear at 900.8, 907.2, and 916.6 eV. This complicated structure of the Ce 3d spectrum is determined by the electronic structure of cerium ions in the initial and final states [3]. Compared with the Ce 3d peak observed for the $nmCeO_2$ and $Co_{0.2}CeO_2$ oxides, the Ce 3d XPS peaks position of $K_{0.1}Co_{0.2}CeO_2$ samples shifted to the lower binding energy. It indicates that the presence of potassium affects the state of cerium oxide, and more Ce^{3+} are produced in the catalyst. As shown in Fig.S3 (c), the O 1s XPS peaks in the $K_{0.1}Co_{0.2}CeO_2$ sample (~528.1 eV) shift to the lower binding energy position compared with the expected value for oxygen in ceria (~529.4 eV). A shoulder peak shows a higher BE (~531.6 eV) attributing to oxygen in the form of -OH or O^- [4,5]. The O^- species is more important for the catalytic combustion of soot.

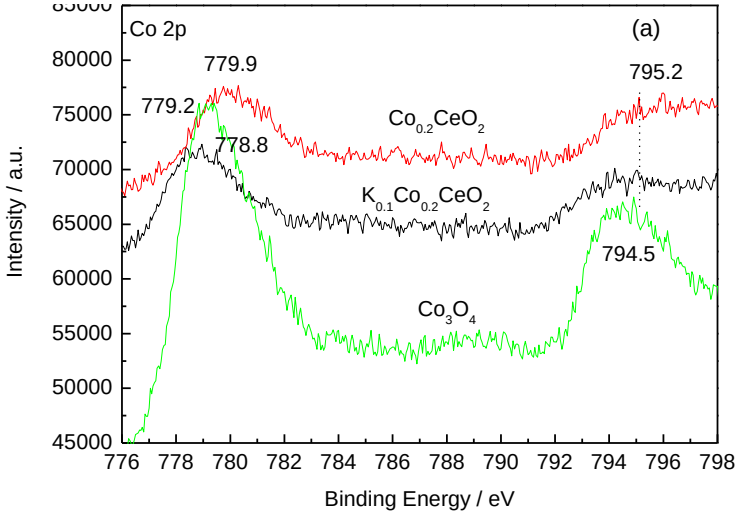

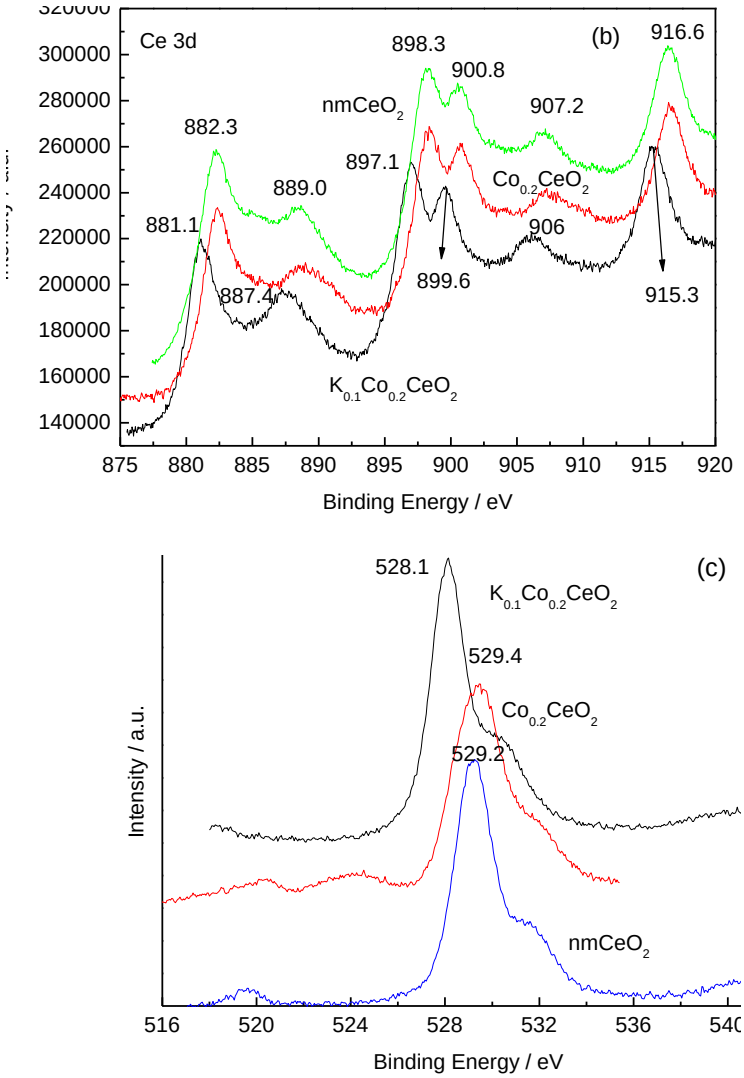

Figure S3: XPS spectra of $nmCeO_2$, $Co_{0.2}CeO_2$ and $K_{0.1}Co_{0.2}CeO_2$ catalysts (a)Co2p (b)Ce3d (c)O1s

Fig. S4 shows the UV-Vis DRS spectra of $K_xCo_{0.2}CeO_2$ catalysts. One strong absorption band centered at 320 nm is attributed to the charge-transfer between the O2p and Ce4f states in O^{2-} and Ce^{4+}. This spectral profile indicates the charge-transfer transition of Ce^{4+} overlaps with the $4f^1 \rightarrow 5d^1$ transition of Ce^{3+} [6]. The bands at 470 nm is due to the formation of Co_3O_4 where a charge transfer via octahedral sites occurs [7], and the other main characteristic bands at 720 nm is ascribed to the transition of d-d electron. These bands become stronger as the potassium content increases.

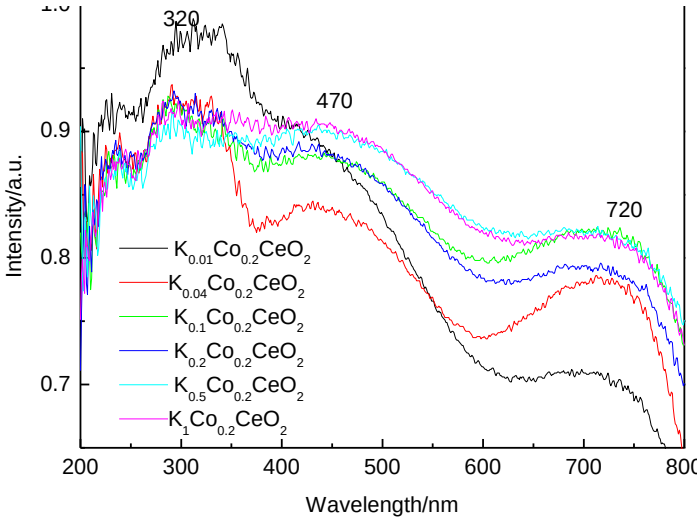

Figure S4: UV-Vis spectra of $K_xCo_{0.2}CeO_2$ catalysts (x=0.01, 0.04, 0.1, 0.2, 0.5, 1)

The Raman spectra of $K_xCo_{0.2}CeO_2$ catalysts are shown in Fig. S5. The absorption peak at around 460 cm^{-1} is attributed to the F_{2g} Raman active mode of fluorite structure in CeO_2 [8]. The presence of low valence ion of potassium and/or cobalt ions in the CeO_2 lattice deforms the structure. It has been reported that this deformation favours oxygen mobility, and thus affects the redox behavior of the material [9, 10]. The absorption peak at 687 cm^{-1} which can be assigned to the stretching vibration of Co-O in the spinel Co_3O_4, indicating that Co_3O_4 crystal phase was present on the catalyst surface [11].

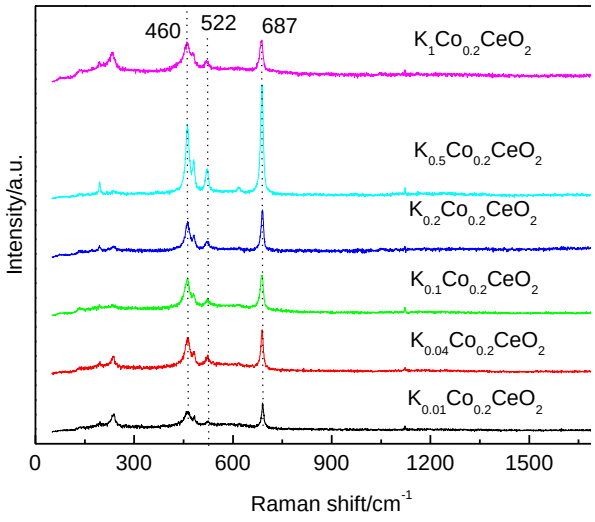

Figure S5: The Raman spectra of $K_xCo_{0.2}CeO_2$ catalysts (x=0.01, 0.04, 0.1, 0.2, 0.5, 1)

Fig. S6 shows the IR spectra of $K_xCo_{0.2}CeO_2$ catalysts. The spectra of the $K_xCo_{0.2}CeO_2$ oxides with low potassium content show strong absorption bands below 600 cm^{-1} and it can be assigned to the Ce-O stretching vibration of cubic fluorite structure in CeO_2 [12]. All samples show two distinct bands at ca. 570 cm^{-1} (ν_1) and 663 cm^{-1} (ν_2) that are due to the stretching

vibrations of the Co-O bond of cobaltic oxide. The ν_1 band is the characteristic vibration of Co^{3+} in octahedral holes and the ν_2 band is attributed to the vibration of Co^{2+} in tetrahedral holes [13].

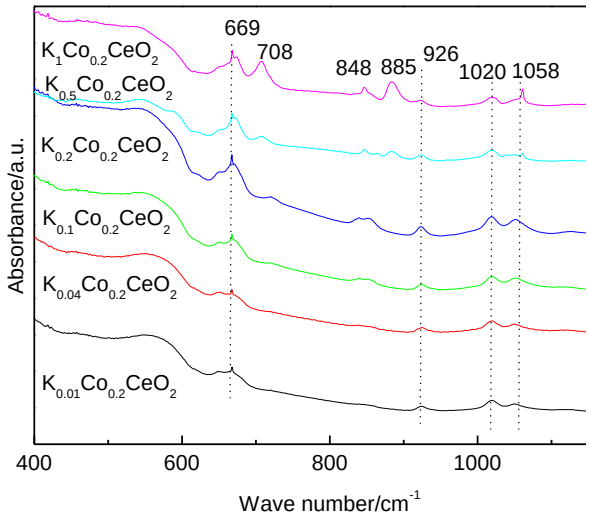

Figure S6: IR spectra of $K_xCo_{0.2}CeO_2$ catalysts. (x=0.01, 0.04, 0.1, 0.2, 0.5, 1)

Catalytic activity measurement:

The catalytic performances of the 3DOM $K_xCo_{0.2}CeO_2$ catalysts were evaluated with a temperature-programmed oxidation (TPO) reaction on a fixed bed tubular quartz system. The reaction temperature was controlled through a PID-regulations system based on the measurements of a K-type thermocouple and varied during each TPO run from 200 to 600 °C at a 2 °C/min rate. The model soot, Printex-U, used in this work was provided by Degussa. Its primary particle size was 25 nm and specific surface was 100 m^2/g. The catalyst and soot were mixed at a mass ratio of 10: 1 with a spatula in order to reproduce the loose contact mode, which is the most representative model of diesel particles flowing through a catalytic filter. Then the mixture placed in the tubular quartz reactor (ϕ = 10 mm) in every test. Reactant gases containing 5% O_2 and 0.2% NO balanced with Ar were passed through a mixture of the catalyst and soot at a flow rate of 50 ml/min (Standard condition). The space velocity of the reaction was about 3000 h^{-1}. The outlet gas compositions coming from the reactor were analyzed with an on-line gas chromatograph (GC, Sp-3420, Beijing) by using FID detectors. The FID was employed to determine CO and CO_2 concentrations after separating these gases over a Porapak N column and converting them to CH_4 over a Ni catalyst at 380 °C. The catalytic activity was evaluated by the values of T_{50} which was defined as the temperatures at which 50% of the soot was oxidized during the TPO procedure. The selectivity to CO_2 formation (S_{CO2}) was defined as that the CO_2 outlet concentration (C_{CO2}) divided by the sum of the CO_2 and CO outlet concentrations, i.e., $S_{CO2} = C_{CO2}/ (C_{CO} + C_{CO2})$. S^m_{CO2} was denoted as the S_{CO2} at the maximum temperature at which soot-burnt rate was the highest. In all TPO experiments, the reaction was not finished until the soot was completely burnt off.

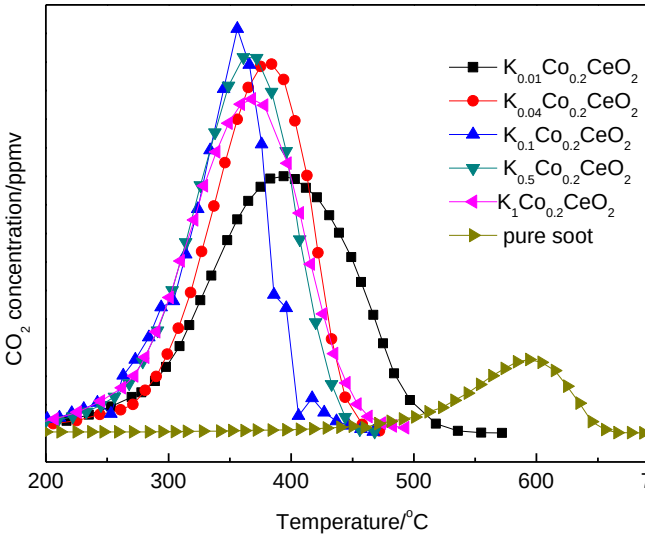

Figure S7: The CO_2 concentration profiles for diesel soot combustion over $K_xCo_{0.2}CeO_2$ catalysts.

TOF measurement:

The TOF (turnover frequency) is defined as the ratio of reaction rate to the active site density of catalysts, and it represents the quantified value of the intrinsic activity. Thus, the catalyst, which has a better redox property, will show a higher intrinsic activity and larger TOF value. To calculate the TOF value, the reaction rate in the kinetic regime is firstly determined by the gas analyses with an on-line gas chromatograph in the isothermal reaction. Because a relatively high feed flow rate (150 ml/min) and low reaction temperature (300 ^oC) are used, the CO_2 signal nearly remain unchanged at a long reaction time. Thus, the reaction rate for soot combustion can be obtained according to the concentration of CO_2 per unit time. More significantly, accurate identification and quantification of the active redox site density is critical for determining TOF values of the catalysts for redox reactions, which is sometimes very difficult for heterogeneous catalysis [14-17]. In this work, we quantified the active oxygen site densities for soot combustion over the $K_xCo_{0.2}CeO_2$ catalysts in the isothermal anaerobic titration by integrating the diminishing rate of CO_2 formation over time after O_2 being removed from the reactant feed. Because the CO_2 is produced from the interaction of the active oxygen and reactant soot, the active site density of catalyst is equal to twice the amounts of CO_2 which can be measured from the shaded areas with the on-line gas chromatograph. Finally, the TOF value could be obtained through calculating the ratio of the reaction rate to the active site density of catalysts. Since the redox ability of $K_{0.1}Co_{0.2}CeO_2$ is the strongest and its TOF value (0.93×10^{-3} s^{-1}) calculated in this work is also quite large, $K_{0.1}Co_{0.2}CeO_2$ catalyst will exhibit an excellent intrinsic activity for soot combustion.

Table S1. Reaction rate, active oxygen (O^*) density, and TOF values for soot combustion with O_2 at 300 ^oC over $K_xCo_{0.2}CeO_2$ catalysts

Catalysts	BET surface area($m^2 \times g^{-1}$)	v[a] (mol s^{-1} $g^{-1} \times 10^{-7}$)	v^*[b] (mol s^{-1} $m^{-2} \times 10^{-9}$)	O^* amount[c] (mol $g^{-1} \times 10^{-4}$)	O^* density[d] (nm^{-2})	TOF[e] ($s^{-1} \times 10^{-3}$)
$K_{0.01}Co_{0.2}CeO_2$	33.8	0.95	2.80	1.12	2.00	0.85
$K_{0.04}Co_{0.2}CeO_2$	35.6	1.18	3.32	1.35	2.28	0.88
$K_{0.1}Co_{0.2}CeO_2$	31.5	2.61	8.28	2.82	5.38	0.93
$K_{0.5}Co_{0.2}CeO_2$	30.2	1.80	5.97	1.99	3.97	0.91
$K_1Co_{0.2}CeO_2$	30.8	1.92	6.15	2.03	4.16	0.92

[a]Reaction rate; [b] the specific reaction rate unit BET surface area; [c] The amount of active redox sites; [d] the density of active redox sites; [e] the ratio of the reaction rate to the active site density.

References:

[1] a) Y. Wei, J. Liu, Z. Zhao, Y. Chen, C. Xu, A. Duan, G. Jiang, H. He, *Angew. Chem. Int. Ed.* 2011, **50**, 2326; b) Y. Wei, J. Liu, Z. Zhao, A. Duan, G. Jiang, C. Xu, J. Gao, H. He, X. Wang, *Enery. Environ. Sci.* 2011, **4**, 2959.

[2] G. Fierro, M. Lo Jacono, M. Inversi, R. Dragone, P. Porta, *Top. Catal.* 2000, **10**, 39.

[3] M. Y. Smirnov, A. V. Kalinkin, A. V. Pashis, A. M. Sorokin, A. S. Noskov, K. C. Kharas, V. I. Bukhtiyarov, *J. Phys. Chem. B* 2005, **109**, 11712.

[4] M. M. Natile, A. Glisenti, *Chem. Mater.* 2005, **17**, 3403.

[5] M. O'Connell, A. K. Norman, C. F. HuÈttermann1, M.A. Morris, *Catal. Today* 1999, **47**, 123.

[6] S. Tsunekawa, T. Fukuda, *J. Appl. Phys.* 1999, **87**, 1318

[7] C. Tang, C. Kuo, M. Kuo, C. Wang, S. Chien, *Appl. Catal. A* 2006, **309**, 37

[8] B.M. Reddy, A. Khan, P. Lakshmanan, M. Aouine, S. Loridant, J. C. Volta, *J. Phys. Chem. B* 2005, **109**, 3355.

[9] B. M. Reddy, A. Khan, Y. Yamada, T. Kobayashi, S. Loridant, J. C. Volta, *J. Phys. Chem. B* 2005, **107**, 11475.

[10] L. Dong, Y. Hu, M. Shen, T. Jin, J. Wang, W. Ding, Y. Chen, *Chem. Mater.* 2001, **13**, 4227.

[11] E. Widjaja, J. T. Sampanthar, X. Han, E. Goh, *Catal. Today* 2008, **131**, 21.

[12] A. Bumajdad, M. I. Zaki, J. Eastoe, L. Pasupulety, *Langmuir* 2004, **20**, 11223.

[13] J. Liu, Z. Zhao, C. Xu, A. Duan, React. Kinet. *Catal. Lett.* 2006, **87**, 107.

[14] S.E. Siporin, R.J. Davis, *J. Catal.* 2004, **225**, 359.

[15] M. Kuriyama, H. Tanaka, S. Ito, T. Kubota, T. Miyao, S. Naito, K. Tomishige, K. Kunimori, *J. Catal.* 2007, **252**, 39.

[16] C.D. Baertsch, S.L. Soled, E. Iglesia, *J. Phys. Chem. B* 2001, **105**, 1320.

[17] H. Nair, C.D. Baertsch, *J. Catal.* 2008, **258**, 1.